



HAL
open science

Elemental depth profiling in transparent conducting oxide thin film by X-ray reflectivity and grazing incidence X-ray fluorescence combined analysis

H. Rotella, B. Caby, Y. Ménesguen, Y. Mazel, A. Valla, D. Ingerle, B. Detlefs, M.-C. Lépy, A. Novikova, G. Rodriguez, et al.

► To cite this version:

H. Rotella, B. Caby, Y. Ménesguen, Y. Mazel, A. Valla, et al.. Elemental depth profiling in transparent conducting oxide thin film by X-ray reflectivity and grazing incidence X-ray fluorescence combined analysis. *Spectrochimica Acta Part B: Atomic Spectroscopy*, 2017, 135, pp.22-28. 10.1016/j.sab.2017.06.011 . cea-02957331

HAL Id: cea-02957331

<https://cea.hal.science/cea-02957331>

Submitted on 5 Oct 2020

HAL is a multi-disciplinary open access archive for the deposit and dissemination of scientific research documents, whether they are published or not. The documents may come from teaching and research institutions in France or abroad, or from public or private research centers.

L'archive ouverte pluridisciplinaire **HAL**, est destinée au dépôt et à la diffusion de documents scientifiques de niveau recherche, publiés ou non, émanant des établissements d'enseignement et de recherche français ou étrangers, des laboratoires publics ou privés.



Distributed under a Creative Commons Attribution 4.0 International License



Elemental depth profiling in transparent conducting oxide thin film by X-ray reflectivity and grazing incidence X-ray fluorescence combined analysis



H. Rotella^a, B. Cabry^a, Y. Ménesguen^b, Y. Mazel^a, A. Valla^c, D. Ingerle^d, B. Detlefs^{a,1}, M.-C. Lépy^b, A. Novikova^b, G. Rodriguez^a, C. Strelid^d, E. Nolot^{a,*}

^a CEA, LETI, MINATEC, 17 rue des Martyrs, Grenoble Cedex 9 38054, France; Univ. Grenoble Alpes, F-38000 Grenoble, France

^b CEA, LIST, Laboratoire National Henri Becquerel, F-91191 Gif-sur-Yvette Cedex, France

^c CEA, LITEN, DTS, INES, 50 avenue du Lac Léman, Le Bourget-du-Lac 73377, France

^d Atominstitut, Vienna University of Technology, Vienna, Austria

ARTICLE INFO

Article history:

Received 13 December 2016

Received in revised form 16 June 2017

Accepted 18 June 2017

Available online 21 June 2017

Keywords:

GIXRF

XRR

Depth profiling

Transparent conducting oxides

ABSTRACT

The optical and electrical properties of transparent conducting oxide (TCO) thin films are strongly linked with the structural and chemical properties such as elemental depth profile. In R&D environments, the development of non-destructive characterization techniques to probe the composition over the depth of deposited films is thus necessary. The combination of Grazing-Incidence X-ray Fluorescence (GIXRF) and X-ray reflectometry (XRR) is emerging as a fab-compatible solution for the measurement of thickness, density and elemental profile in complex stacks. Based on the same formalism, both techniques can be implemented on the same experimental set-up and the analysis can be combined in a single software in order to refine the sample model. While XRR is sensitive to the electronic density profile, GIXRF is sensitive to the atomic density (i. e. the elemental depth profile). The combination of both techniques allows to get simultaneous information about structural properties (thickness and roughness) as well as the chemical properties. In this study, we performed a XRR-GIXRF combined analysis on indium-free TCO thin films (Ga doped ZnO compound) in order to correlate the optical properties of the films with the elemental distribution of Ga dopant over the thickness. The variation of optical properties due to annealing process were probed by spectroscopic ellipsometry measurements. We studied the evolution of atomic profiles before and after annealing process. We show that the blue shift of the band gap in the optical absorption edge is linked to a homogenization of the atomic profiles of Ga and Zn over the layer after the annealing. This work demonstrates that the combination of the techniques gives insight into the material composition and makes the XRR-GIXRF combined analysis a promising technique for elemental depth profiling.

© 2017 Elsevier B.V. All rights reserved.

1. Introduction

One of the challenges in the optoelectronic devices is to find an acceptable compromise between the need to increase the light emitting/absorbing area and the need for low series resistance of the metal contact grid [1]. The use of transparent conducting oxides (TCOs) allows to achieve this compromise. Heretofore the class of TCO materials have been dominated by ITO (indium tin oxide, an In-rich alloy of indium oxide and tin oxide). However, due to the

expected scarcity of indium, efforts are underway to develop indium-free TCOs for the above-mentioned devices. ZnO heavily doped with Ga (GZO) is becoming a very attractive candidate for future generation TCOs [2].

ZnO belongs to groups II–VI semiconductors, featuring a wide band gap (3.3 eV) at room temperature [3]. ZnO has been widely used in photoelectric applications [4–7]. Pure ZnO is an intrinsic n-type semiconductor and the main sources of electrons are oxygen vacancies and interstitial zinc atoms [8]. However, the effects of both sources are weakened at room temperature [9]. As a result, the optical and electrical properties of ZnO can only be enhanced through doping [10].

The physical properties of heavily doped thin layers, such as optical and electrical behaviors are strongly dependent on the

* Corresponding author.

E-mail address: emmanuel.nolot@cea.fr (E. Nolot).

¹ New address: ESRF, 71, Avenue des Martyrs, Grenoble 38043, France.

structural (thickness, density, roughness) and chemical (elemental depth profiles) properties. In our study, we focused on ZnO thin films doped with Ga. We studied the effect of the doping on the optical and electrical properties before and after the annealing process using spectroscopic ellipsometry and Hall effect measurements. In order to interpret the physical behavior of the films, we performed a deep structural and chemical analysis.

We used non-destructive methods in order to characterize the systems at an industrial level. Recently the combination of two techniques, X-ray reflectometry (XRR) and grazing-incidence X-ray fluorescence (GIXRF) has become a strong candidate for this characterization [11]. Both techniques use similar measurement procedures and the same fundamental physical principles can be used to analyze the data. The experimental acquisition require a parallel monochromated incident beam. From the theoretical point of view, both techniques are based on the same recursive Parratt's formalism [12]. In 1954, Parratt presented the modulation effect of the electromagnetic field as a function of the incident angle based on reflection, refraction and interferences at a flat interface. He proposed a recursive method for the calculation of the reflected part of the beam (XRR). Based on the same recursive method, in 1991, De Boer presented a theoretical formulation for the fluorescence emitted (GIXRF) from layered samples based on the calculation of the derivative of the Poynting vector through the determination of the reflection and transmission coefficients [13].

The XRR analysis is a well-known interface-sensitive analytical technique used to characterize surfaces, thin films and multilayers. Basically, the technique is to reflect an X-ray beam on a sample (film + substrate) and to measure the intensity of the reflected beam in the specular direction while varying the incident beam angle in the grazing range (θ). When the interface between the film and the substrate is not perfectly sharp, *i.e.* has an average electron density profile, then the specular reflected intensity will deviate from the Fresnel's law reflectivity prediction. The deviation can be analyzed to obtain the electronic density profile normal to the surface as well as the film thickness and the interfaces roughnesses [14]. Prior knowledge of the chemical composition of each layer is then necessary to obtain the mass density of the respective layer.

The GIXRF analysis is a powerful technique for elemental depth profiling of thin layers. The basic concept of this technique is to measure the fluorescence signal emitted by the elements present in the sample as a function of angle of incidence of the X-rays. In the grazing angle range, the incident and the reflected beam interfere creating an X-ray standing wave (XSW) field with locally dependent electric field fluctuations [15]. The emitted fluorescence signal is thus amplified by the intensity of the XSW field at a given depth resulting in a strong dependence on the elemental depth profile (*i.e.* atomic density).

The primary XRF intensity per unit of time by atoms of a particular element a in a layer j of a thickness d_j can be represented by the following equation [16]:

$$I_{aj} = \frac{1}{I_0} C_{aj} \frac{\tau_{a\lambda}}{\mu_{j\lambda}/\rho_j} J_{a\lambda} \omega_a g_a \exp\left(-\sum_{n=1}^{j-1} \frac{\mu_{na} d_n}{\sin \phi_d}\right) S \times \int_0^{d_j} dz \left(-\frac{\partial P_{jz}}{\partial z}\right) \exp\left(-\frac{\mu_a z}{\sin \phi_d}\right), \quad (1)$$

where I_0 is the incident photon energy (hc/λ , where h is Planck's constant, c the velocity of the light in vacuum and λ the wavelength), C_{aj} the mass fraction of element a in layer j , $\tau_{a\lambda}$ the photoelectric part of the mass absorption coefficient for element a at wavelength λ , $\mu_{j\lambda}$ the linear absorption coefficient of the incident radiation in layer j , ρ_j the atomic density of layer j , $J_{a\lambda}$ the absorption jump factor at wavelength λ for the considered shell of element a , ω_a the fluorescence yield, g_a the relative emission rate, μ_{na} the linear absorption

coefficient of the considered fluorescence of element a in layer n , d_n the layer n thickness, S the irradiated detected sample area, ϕ_d the detector angle, P_{jz} the z component of the Poynting vector and μ_{ja} the linear absorption coefficient of the considered fluorescence of element a in layer j . One can note the link between the different absorption coefficients (linear and mass) producing correlation effects between the fit parameters during the analysis.

The analysis of the GIXRF signal gives the information of the atomic density over the overall thickness linked to the elemental depth profile. However, this technique does not provide an unambiguous depth profile reconstruction in terms of mass density and thickness.

While both techniques used independently require prior knowledge of the sample, combining them gives access to a better characterization of the system in terms of thickness, roughness and mass density profile by combining the electronic and the atomic density profiles [17]. In this work we demonstrate how the GIXRF/XRR combined strategies apply for non-destructive characterization of the depth-dependent properties in gallium-doped zinc oxide thin layered films, and how the optical properties of this advanced indium-free TCO relate to the XRR/GIXRF-deduced gallium profile in the film. In Ga-doped ZnO compounds, the electronic density is not significantly impacted by the substitution of Zn by Ga. On the contrary, the atomic density is very sensitive to the presence of Ga atoms although the atomic numbers (Z) of Zn and Ga are very close. The characterized structural and chemical properties give a better insight into the physical properties of the films and allow to interpret the observed optical properties.

2. Experimental

2.1. Sample preparation

Ga doped ZnO thin films on SiO₂ (500 nm)//Si substrate were prepared industrially. The SiO₂ layer was thermally deposited on Si(100) substrate. We use such SiO₂//Si substrate in order to control the thickness as well as the oxidation state of the oxide layer. We deposited 2.5 at.% Ga doped ZnO (noted Ga_{0.05}Zn_{0.95}O) 15 nm thin films on 8 inches wafers. One pair of samples of 2 cm × 4 cm (close to each other) was cut on the wafer and one specimen of the pair was then annealed under industrial conditions. The annealing conditions were optimized in order to achieve the best physical properties according to reference [18]. As a reference sample, we prepared a pure 20 nm thick ZnO thin film deposited on a SiO₂ (500 nm)//Si substrate using the atomic layer deposition (ALD) technique in order to control the thickness and the composition of the film as well as to limit the roughnesses at the interfaces.

2.2. Instrumentation

The spectroscopic ellipsometry data have been acquired using a Woollam M2000 rotating compensator ellipsometer which features automated variable angle of incidence capability (VASE), 193–1700 nm spectral range and spot size in the mm range.

Hall effect measurements were done with an Ecopia HMS5000 system at 300 K applying a magnetic field of 0.55 T to obtain the carrier density using Van der Pauw method [19].

The structural properties probed by XRD were examined using a Panalytical X'Pert Pro MRD diffractometer with a monochromated parallel beam Cu K α excitation using a $\theta/2\theta$ configuration.

The XRR and GIXRF data were acquired simultaneously using a dedicated instrument. Recently, the National Henri Becquerel Laboratory (CEA) has acquired a specific set-up to perform the combined XRR-GIXRF analysis [20]. It has been implanted on the Metrology beamline at the French synchrotron SOLEIL (Saclay), the set-up can be used in the X-UV energy range (45 eV to 1.9 keV) as well as in

the hard X-ray energy range (3 to 35 keV). The analysis chamber is composed of a 7-axis goniometer allowing a fine alignment of the sample in the chamber with respect to the incoming beam and its rotation during measurement. Two detectors complete the set-up, including a diode to record the XRR signal and a HPGe spectrometer from OXFORD Instruments to acquire the fluorescence intensity. The environment of the measurement is maintained under vacuum at $P < 10^{-6}$ mbar. Two sets of slits, placed in the incoming beam and before the XRR detector are used in order to limit the divergence and eliminate the off-specular signal. The XRR measurement is performed in a $\theta/2\theta$ configuration. The fluorescence detector, including a collimator, is placed at 90° with respect to the sample surface. The GIXRF measurement is performed by rotating the sample by the θ angle identical to the one in the XRR measurement. Due to a fixed incident beam, the rotation of the sample during the measurement implies an evolution of the solid angle of detection which affects the collected fluorescence intensity by the factor S , the irradiated detected sample area (see Eq. (1)) [16,21].

Finally, the destructive chemical depth profiling analysis has been realized using a PPTOFMS from Horiba Jobin-Yvon [22]. The instrument combines a plasma source (pulsed radio-frequency glow discharge) for sputtering and ionization of the sample coupled with an orthogonal time-of-flight mass spectrometer.

2.3. Methodology

In this study, the combined XRR-GIXRF analysis has been performed in the hard X-ray range using a 10.8 keV energy for the incident beam. The choice of this measurement energy was made to be sufficiently above the K-edges of elements of interest present in the system, i.e. 10.367 keV for Ga and 9.659 keV for Zn to enhance the fluorescence signal. We recorded the XRR data from 0° to 1° with an angular step of 0.005° . The XRF spectra were acquired on the same range but with a larger angular step of 0.01° . We analyzed each spectrum with PyMca software [23] using batch processing, resulting in the dependence of the integrated intensity of each element line of interest with the incident angle. Fig. 1 represents the sum of the spectra recorded along the θ range on the as-deposited 15 nm thick Ga doped ZnO sample analyzed using PyMca software. The background was simulated using a strip background model implemented in the software. This approach is consistent with the hard X-ray regime used in this analysis. We clearly observe the K_α and K_β lines of Zn and Ga which can be easily deconvoluted. The peak at 10.8 keV is the elastic scattering peak. The presence of the three elements Cr, Fe and Ni comes from the analysis chamber itself.

The XRR-GIXRF combined analysis can be performed following two distinct approaches. A reference-free analysis approach may be

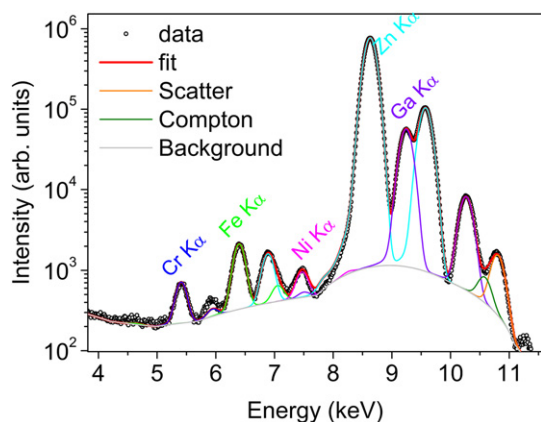


Fig. 1. Sum of the spectra recorded at 10.8 keV along the θ range on the as-deposited 15 nm thick Ga doped ZnO sample analyzed using the PyMCA software.

used if one has access to the calibration of the whole system. This implies a preliminary detector calibration in terms of geometrical parameters and efficiency as well as a characterization of the incident beam including the intensity, the shape and the divergence [24,25]. Otherwise, the second approach is the use of a reference sample containing the same element in order to define the geometrical factor and the detector response depending on the fluorescence emission line. In our study we chose to measure a 20 nm ZnO sample deposited by the ALD technique. This deposition technique allows to get a smooth sample (low roughness) and a good control of the composition and the thickness of the film. A classic XRR analysis is sufficient to characterize the reference sample. The K_α emission energy of Ga and Zn are very close, we can expect a constant response in the efficiency of the detector between both elements. Thus, the ZnO thin film is a good candidate as reference sample for both elements.

We performed the combined analysis on this sample using JGIXA software [26,27] in order to get the geometrical parameters values of the experiment, including the detected area (factor S in Eq. (1)) and the XRR and the XRF divergence factors. We then proceeded to the combined analysis of both samples of interest while fixing the set of instrumental parameter. The starting models were composed of one layer of $\text{Ga}_{0.05}\text{Zn}_{0.95}\text{O}$ of 15 nm over an infinite substrate of SiO_2 with a set of expected parameters. The optimization is performed in JGIXA using a differential evolution algorithm [28].

3. Results and discussion

3.1. Spectroscopic ellipsometry

The optical responses of both as-deposited and annealed samples are represented in Fig. 2 and compared with the ZnO reference sample response. The ψ and δ spectra (not shown here) are recorded over a wide spectral range from UV to Near-IR wavelength [193–1700 nm] at several incident angles. The dielectric function of the ZnO thin film was modeled by combining one Drude oscillator with one Tauc-Lorentz and one gaussian oscillators [29]. The dielectric function of the TCO thin films were then extracted using the previous model only by fitting the positions and the amplitudes of the oscillators.

Qualitatively, we observe a strong influence on the optical properties of the presence of Ga dopant in as-deposited ZnO thin film. A signature of crystalline defects appears around 3.2 eV certainly due to a lack of homogeneity. The contribution of plasma excitation (free electrons) to the dielectric function can be observed in the visible and near-infrared spectra region but a further analysis in the infra-red region may be needed to validate the hypothesis.

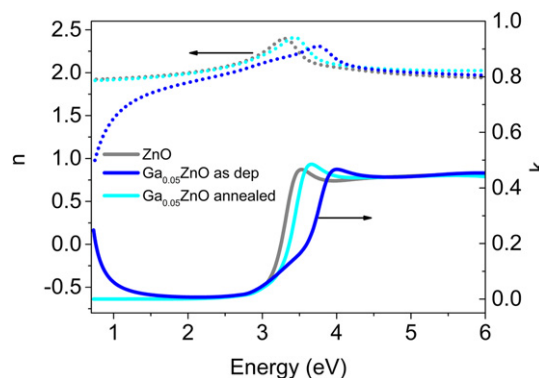


Fig. 2. Refractive index and extinction coefficient of as-deposited and annealed Ga doped ZnO samples compared with a ZnO reference sample.

The annealing process slightly decreases these effects and the optical parameters are closer to the one of ZnO, although significant blue shift in the optical absorption edge remains.

In heavily doped polycrystalline semiconductor such as GZO compound, the main mechanisms responsible of the optical response are the following [30]:

- i Burstein-Moss (BM) shift
- ii Atomic structure distortions and reconstructions
- iii Alloying effect (orbital hybridization)
- iv Exciton effects

In the first approximation the blue shift of the optical band gap can be explained mostly by the BM shift. It is directly correlated to the amount of free-carrier concentration (n) according to the following relation given by Burstein [31]:

$$\Delta E_g \simeq \frac{h^2}{8m^*} \left(\frac{3}{\pi}\right)^{\frac{2}{3}} n^{\frac{2}{3}}, \quad (2)$$

where ΔE_g is the energy band gap widening, n the carrier concentration, h the Planck's constant, and m^* the electron effective mass in the conduction band. In the case of ZnO semiconductor $m^* = 0.28m_e$ [32].

In a band-edge absorption region, the absorption coefficient α of the TCO thin films is approximated by $\alpha E = A(E - E_g)^{1/2}$. Assuming a direct band gap transition, we can thus extract the optical gap value E_g by plotting $(\alpha E)^2$ versus photon energy [33]. The α spectra can be obtained directly from the k spectra using the formula $\alpha = 4\pi k/\lambda$.

Fig. 3 shows the $(\alpha E)^2$ plot for both samples as-deposited and annealed Ga doped ZnO in comparison with ZnO thin film. We determined the optical gap for the three samples by linear extrapolation (solid lines) and E_g was estimated from the intercept at $(\alpha E)^2 = 0$. ZnO thin film presents an optical gap at 3.2 eV in good agreement with the reported value in the literature [34]. The presence of Ga dopant in ZnO thin film increased the optical gap to 3.6 eV. The annealing process decreased the optical gap to 3.4 eV. The increase in the optical band gap correlates with an increased in electron concentration according to Eq. (2). The annealing process removes a part of the electrons occupying the energy states above the bottom of the conduction band, thus decreasing both the optical band gap and the electron density. We performed Hall measurement on both samples in order to extract the electron density before and after the annealing process. The measured values are $8.0 \times 10^{20} \text{ cm}^{-3}$ and $2.9 \times 10^{20} \text{ cm}^{-3}$ for the as-deposited and annealed sample respectively. The calculated band gap widenings from these values given by the Eq. (2),

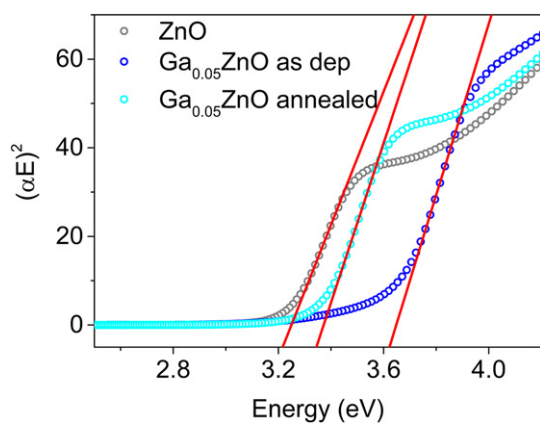


Fig. 3. $(\alpha E)^2$ versus photon energy for the three samples: as-deposited and annealed Ga doped ZnO samples compared with a ZnO reference sample. The extraction of the optical gap value is given by extrapolating the intercept at $(\alpha E)^2 = 0$.

are 1.08 eV and 0.55 eV, respectively. Experimentally, the band gap widenings are quite slighter, 0.4 eV and 0.2 eV respectively. Although the evolution and the order of magnitude are similar, the difference between calculated and experimental values can be explained by other contributions in the band gap widening such as defects which tend to decrease the BM effect [35].

In order to further interpret the annealing effect on the optical properties of Ga-doped ZnO thin film, we perform an X-ray analysis of both samples including diffraction, reflectivity and fluorescence.

3.2. XRD and XRR analyses

Fig. 4 presents the diffracted patterns of both samples around the (002) ZnO reflection. GZO thin films are polycrystalline. In this work, only the (002) reflection peak is considered. We clearly observe a decrease in the lattice parameter after the annealing process.

A preliminary fitting procedure was performed on the XRR data only using a genetic algorithm with Leptos[®] software. We started the fitting procedure with a 15 nm $\text{Ga}_{0.05}\text{Zn}_{0.95}\text{O}$ monolayer model for both samples. Fig. 5 represents the simulated and recorded data on both samples after the refinement procedure. The inset represents the mass density profile for both as-deposited (A) and annealed (B) samples. The fitted sample parameter results are reported in Table 1.

The total thickness of the film after the annealing process has shrunk. Indeed the total thickness of the as-deposited sample is around 18 nm while the annealed sample is only 15 nm thick. While the fit was adequate for the annealed sample, this model was not adapted for the as-deposited sample. The best model calculation of XRR data of the as-deposited sample required the addition of a low density thin surface layer (compared to the reported value in the literature for doped ZnO compound [34]). We applied the same composition for both layers assuming that the effect on XRR signal is weak. The annealed sample presents a mass density close to the reported value of bulk ZnO. One should note that the mass density profile is deduced from the electronic density profile using the given composition $\text{Ga}_{0.05}\text{Zn}_{0.95}\text{O}$.

Low density top layer in the as-deposited sample can be related to an elemental profile in the film as well as defaults such as voids or vacancies in the GZO matrix. According to the XRR results, the annealing process seems to homogenize the film and decrease the total thickness. This observation is coherent with the XRD measurement which reveals a reduction of the lattice parameter after the annealing process. Indeed the presence of defects such as vacancies in oxide thin films tends to expand the lattice [36,37]. In order to verify the hypothesis of a more homogeneous annealed film in terms of elemental profile a combined XRR-GIXRF analysis has been performed.

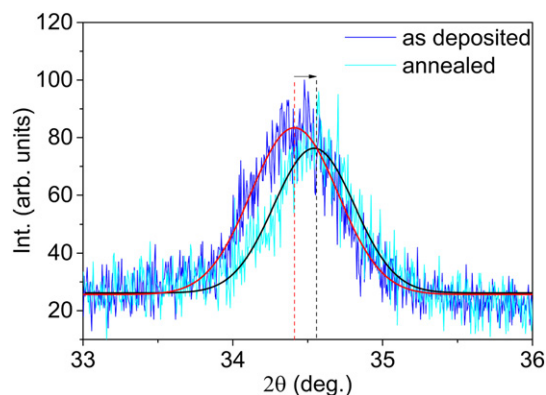


Fig. 4. XRD patterns along the 002 reflection of ZnO of as-deposited and annealed Ga doped ZnO samples.

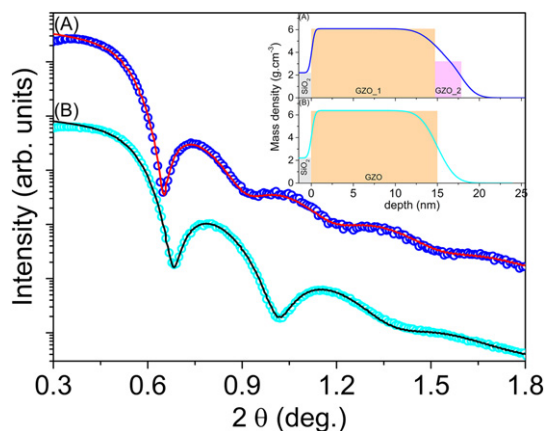


Fig. 5. XRR measurements (open circles) and simulated curves (solid lines) after refinement procedure of both as-deposited (A) and annealed (B) samples. The inset represents the electronic density profile for both samples. The fitted result parameters are reported in Table 1.

3.3. Combined analysis

The principle of the combined analysis is to use only one model to represent both XRR and GIXRF data. In our case, we extracted the angular dependence of the Ga and the Zn K_{α} lines in the XRF spectra. The data were processed using JGIXA software. The instrumental parameters were set to previously determined values by the procedure detailed in Section 2.3 on the 20 nm thick ZnO reference sample. We started the fitting procedure with the models obtained from the previous XRR analysis for both samples, as-deposited and annealed, respectively.

Qualitatively we observe on the as-deposited samples that, although the fit is in good agreement for the XRR data, neither the Zn nor the Ga GIXRF signal is well represented by the XRR model (not shown here). This reveals that not only there is a density profile but also the Zn and the Ga present an atomic gradient over the thickness of the film.

Similarly, the annealed sample presents discrepancies in the simulation of GIXRF data for Ga K_{α} line by the XRR model (not shown here), although the simulated GIXRF signal for the Zn K_{α} line is satisfying. This underlines our conclusion that in the case of the annealed sample the Zn atomic profile is more homogeneous.

In order to integrate an elemental profile in our models, using JGIXA software we subdivided the layers in discrete thin layers with defined thickness (3 nm) and released the constraint on the elemental concentration of Ga, Zn and O. The recorded data and the simulated curves of the combined analysis for both as-deposited (A) and annealed (B) samples are shown in Figs. 6 and 7, respectively. The extracted elemental profiles are represented in Fig. 8.

In the combined analysis we assume a substitutional doping meaning that the total concentration of Ga, Zn and O atoms at all depths in the film is fixed to 1. With this hypothesis the as-deposited sample shows a strong elemental gradient over the layer. We observe an increase of Zn concentration in the top layers of the film, especially over the first 3 nm, accompanied by a decrease of Ga content. The results of the combined analysis on both samples

Table 1
Fitting results of the XRR data refinement for both samples as-deposited (A) and annealed (B) performed using Leptos® software.

Sample	Model	Thickness (nm)	Density ($\text{g}\cdot\text{cm}^{-3}$)	Roughness (nm)
A	GZO_2	3.2(9)	3.21(9)	1.4(5)
	GZO_1	14.7(9)	6.08(2)	1.8(9)
B	GZO	15.0(1)	6.38(7)	1.7(1)

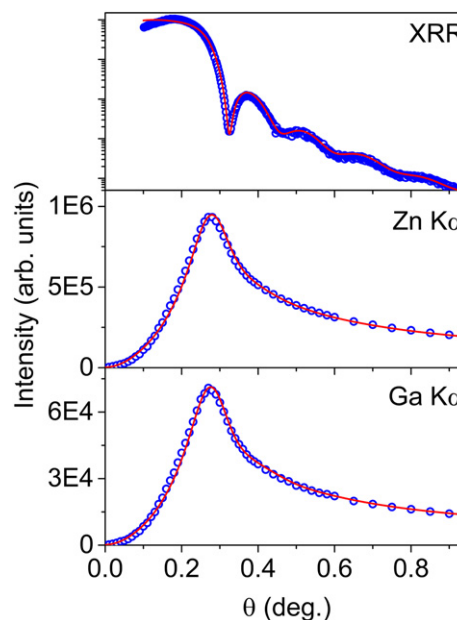


Fig. 6. XRR-GIXRF measurements (open circles) and simulated curves (solid lines) after refinement procedure of the as-deposited sample A. The fitted result parameters are presented in Fig. 8.

confirm homogenization of the composition after the annealing process. Although a slight elemental profile remains in the annealed sample, we observe a higher concentration of Ga in the first 3 nm concomitant with a decrease in the Zn concentration.

In parallel to the combined XRR-GIXRF analyses, we performed a destructive chemical depth profiling analysis of the samples using a PPTOFMS from Horiba Jobin-Yvon [22]. Ion Beam Ratios for Ga, Zn and Si are shown in Fig. 9 [38]. Analysis time was converted to depth assuming constant sputtering rate. While the as-deposited sample exhibits a Zn-rich surface, Zn and Ga clearly homogenize throughout the layer during annealing process. Measured and simulated

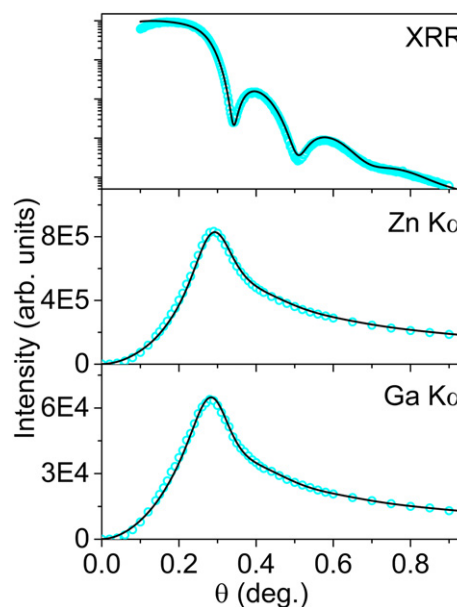


Fig. 7. XRR-GIXRF measurements (open circles) and simulated curves (solid lines) after refinement procedure of the annealed sample B. The fitted result parameters are presented in Fig. 8.

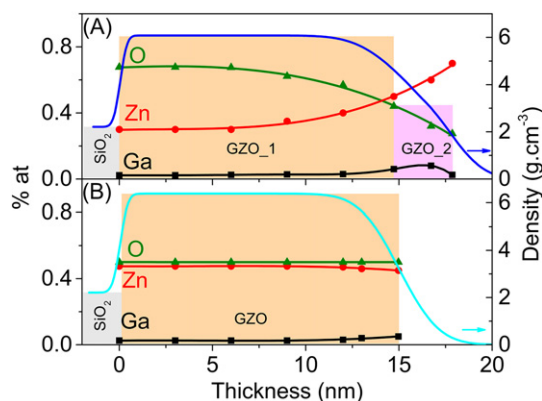


Fig. 8. Atomic and density profile for both as-deposited (A) and annealed (B) samples deduced from XRR-GIXRF combined analysis.

profiles are consistent and tend to strengthen the credibility of the XRR-GIXRF combined analysis.

3.4. Discussion

The spectroscopic ellipsometry measurement on the as-deposited Ga doped ZnO thin films shows the presence of defects and an increase in the optical band gap associated with an increase of the charge electron density. The XRR analysis reveals a top layer with a very low mass density related to defects and elemental gradient. The XRR-GIXRF combined analysis confirms an elemental gradient of Ga and Zn over the depth which has been validated by a destructive technique. The annealing process seems to homogenize the film. The thickness shrinking observed after annealing is coherent with a decrease of the lattice parameter but is also enhanced by the increased density due to an atomic rearrangement.

According to the XRR analysis, the density profile of the annealed sample is well represented by a monolayer, although the XRR-GIXRF combined analysis reveals a slight Ga and Zn elemental profile with an increase of Ga at the surface. This can be explained by the fact that the compound of Ga_2O_3 is thermodynamically favored compared to ZnO. Indeed considering the annealing condition, the Gibbs energy of the Ga_2O_3 is below the ZnO one [39]. During the annealing process, the excess of oxygen atoms at the surface due to air oxidation will favorably react with the Ga atoms, increasing the amount of Ga

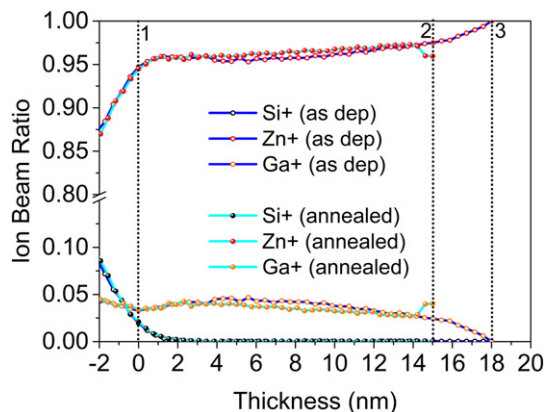


Fig. 9. Relative ion beam ratio of Zn, Ga and Si atoms for both as-deposited and annealed samples measured by PPTOFMS technique. The dot lines represent the interface between the SiO_2 substrate and the films (1) and the surface of the annealed sample (2) and the as-deposited sample (3).

at the surface. The homogenization of the films is accompanied by a decrease of the optical band gap as observed with the SE measurements which is related to a diminution of the charge carrier density. The amount of defects in the gap decreases as well which is coherent with homogeneous mass density and atomic profiles.

4. Conclusions

In this study we correlated and explained the optical properties of Ga doped ZnO as-deposited and annealed thin films with the mass density and the atomic profiles by performing a non-destructive XRR-GIXRF combined analysis. We found that the annealing process affects the optical properties by a homogenization of the mass density and the elemental profile over the thickness. We demonstrate that the XRR-GIXRF combined analysis technique is a powerful analysis for elemental depth profiling on thin layers. More specifically, this measurement can distinguish the presence of elements with very close atomic numbers (Ga and Zn) and a weak effect on the electronic density. Moreover the non-destructive nature makes this analysis a suitable candidate for industrial process control which can be part of R&D production.

Acknowledgments

This project is part of the European ThinErgy project (ENG53-ThinErgy) and has been supported by the European Metrology Research Programme (EMRP) Project ENG53-ThinErgy which is jointly funded by the EMRP participating countries within EURAMET and the European Union.

References

- [1] H. Liu, V. Avrutin, N. Izyumskaya, U. Özgür, H. Morkoç, Transparent conducting oxides for electrode applications in light emitting and absorbing devices, *Superlattice. Microst.* 48 (2010) 458–484. <http://dx.doi.org/10.1016/j.spmi.2010.08.011>.
- [2] H. Mahdhi, Z.B. Ayadi, S. Alaya, J. Gauffier, K. Djessas, The effects of dopant concentration and deposition temperature on the structural, optical and electrical properties of Ga-doped ZnO thin films, *Superlattice. Microst.* 72 (2014) 60–71. <http://dx.doi.org/10.1016/j.spmi.2014.04.013>.
- [3] R.D. Vispute, V. Talyansky, S. Choopun, R.P. Sharma, T. Venkatesan, M. He, X. Tang, J.B. Halpern, M.G. Spencer, Y.X. Li, L.G. Salamanca-Riba, A.A. Iliadis, K.A. Jones, Heteroepitaxy of ZnO on GaN and its implications for fabrication of hybrid optoelectronic devices, *Appl. Phys. Lett.* 73 (1998) 348–350. <http://dx.doi.org/10.1063/1.121830>.
- [4] Z. You, G. Hua, Electrical, optical and microstructural properties of transparent conducting GZO thin films deposited by magnetron sputtering, *J. Alloys Compd.* 530 (2012) 11–17. <http://dx.doi.org/10.1016/j.jallcom.2012.03.078>.
- [5] Q. Zhang, C.S. Dandeneau, X. Zhou, G. Cao, ZnO nanostructures for dye-sensitized solar cells, *Adv. Mater.* 21 (2009) 4087–4108. <http://dx.doi.org/10.1002/adma.200803827>.
- [6] P.-H. Lei, M.-J. Ding, Y.-C. Lee, M.-J. Chung, Textured zinc oxide prepared by liquid phase deposition (LPD) method and its application in improvement of extraction efficiency for 650 nm resonant-cavity light-emitting diode (RCLED), *J. Alloys Compd.* 509 (2011) 6152–6157. <http://dx.doi.org/10.1016/j.jallcom.2011.03.039>.
- [7] J. Chen, J. Li, J. Li, G. Xiao, X. Yang, Large-scale syntheses of uniform ZnO nanorods and ethanol gas sensors application, *J. Alloys Compd.* 509 (3) (2010) 740–743. <http://dx.doi.org/10.1016/j.jallcom.2010.09.043>.
- [8] A. Janotti, C.V. de Walle, Native point defects in ZnO, *Phys. Rev. B* 76 (2007) 165202. <http://dx.doi.org/10.1103/PhysRevB.76.165202>.
- [9] M. McCluskey, S. Jokela, Defects in ZnO, *J. Appl. Phys.* 106 (2009) 071101. <http://dx.doi.org/10.1063/1.3216464>.
- [10] Y.-S. Lee, Y.-C. Peng, J.-H. Lu, Y.-R. Zhu, H.-C. Wu, Electronic and optical properties of Ga-doped ZnO, 570, *Thin Solid Films* 570 (Part B) (2014) 464–470. <http://dx.doi.org/10.1016/j.tsf.2014.04.037>.
- [11] J. Lubeck, B. Beckhoff, R. Fliegau, I. Holfelder, P. Hönicke, M. Müller, B. Pollakowski, F. Reinhardt, J. Weser, A novel instrument for quantitative nanoanalytics involving complementary X-ray methodologies, *Rev. Sci. Instrum.* 84 (2013) 045106. <http://dx.doi.org/10.1063/1.4798299>.
- [12] L. Parratt, Surface studies of solids by total reflection of X-rays, *Phys. Rev.* 95 (1954) 359–369. <http://dx.doi.org/10.1103/PhysRev.95.359>.
- [13] D.K.G de Boer, Glancing-incidence X-ray fluorescence of layered materials, *Phys. Rev. B* 44 (1991) 498–511. <http://dx.doi.org/10.1103/PhysRevB.44.498>.
- [14] J. Als-Nielsen, D. McMorrow, *Elements of Modern X-ray Physics*, Wiley, 2001.

- [15] A. von Bohlen, Total reflection X-ray fluorescence and grazing incidence X-ray spectrometry - tools for micro- and surface analysis, *Spectrochim. Acta, Part B* 64 (2009) 821–832. <http://dx.doi.org/10.1016/j.sab.2009.06.012>.
- [16] D.K.G. De Boer, Angular dependence of X-ray fluorescence intensities, *X-Ray Spectrom.* 18 (1989) 119–129. <http://dx.doi.org/10.1002/xrs.1300180309>.
- [17] B. Cabry, F. Brigidi, D. Ingerle, E. Nolot, G. Pepponi, C. Strelti, L. Lutterotti, A. André, G. Rodriguez, P. Gergaud, M. Morales, D. Chateigner, Study of annealing-induced interdiffusion in $\text{In}_2\text{O}_3/\text{Ag}/\text{In}_2\text{O}_3$ structures by a combined X-ray reflectivity and grazing incidence X-ray fluorescence analysis, *Spectrochim. Acta, Part B* 113 (2015) 132–137. <http://dx.doi.org/10.1016/j.sab.2015.09.008>.
- [18] K. Yen, C. Chiu, C. Li, C. Chou, P. Lin, T. Chen, T. Lin, J. Gong, Performance of InGaN/GaN MQW LEDs using Ga-doped ZnO TCLs prepared by ALD, *IEEE Photon. Technol. Lett* 24 (23) (2012) 2105–2108. <http://dx.doi.org/10.1109/LPT.2012.2220537>.
- [19] A. Valla, P. Carroy, F. Ozanne, D. Muñoz, Understanding the role of mobility of ITO films for silicon heterojunction solar cell applications, *Sol. Energy Mater. Sol. Cells* 157 (2016) 874–880. <http://dx.doi.org/10.1016/j.solmat.2016.08.002>.
- [20] Y. Ménesguen, B. Boyer, H. Rotella, J. Lubeck, J. Weser, B. Beckhoff, D. Grötzsch, B. Kanngießer, A. Novikova, E. Nolot, M.C. Lépy, CASTOR, a new instrument for combined XRR-GIXRF analysis at SOLEIL, *X-Ray Spectrom.* (2017) <http://dx.doi.org/10.1002/xrs.2742>.
- [21] W. Li, J. Zhu, X. Ma, H. Li, H. Wang, K.J.S. Sawhney, Z. Wang, Geometrical factor correction in grazing incident X-ray fluorescence experiment, *Rev. Sci. Instrum.* 83 (2012) 053114. <http://dx.doi.org/10.1063/1.4722495>.
- [22] A. Tempez, S. Legendre, P. Chapon, Depth profile analysis by plasma profiling time of flight mass spectrometry, *Nucl. Inst. Methods Phys. Res. B* 332 (2014) 351–354. 21st International Conference on Ion Beam Analysis. <http://dx.doi.org/10.1016/j.nimb.2014.02.094>.
- [23] V. Solé, E. Papillon, M. Cotte, P. Walter, J. Susini, A multiplatform code for the analysis of energy-dispersive X-ray fluorescence spectra, *Spectrochim. Acta B At. Spectrosc.* 62 (2007) 63–68. <http://dx.doi.org/10.1016/j.sab.2006.12.002>.
- [24] B. Beckhoff, Reference-free X-ray spectrometry based on metrology using synchrotron radiation, *J. Anal. At. Spectrom.* 23 (2008) 845–853. <http://dx.doi.org/10.1039/B718355K>.
- [25] P. Hönicke, B. Detlefs, M. Müller, E. Darlatt, E. Nolot, H. Grampeix, B. Beckhoff, Reference-free, depth-dependent characterization of nanolayers and gradient systems with advanced grazing incidence X-ray fluorescence analysis, *Phys. Status Solidi A* 212 (2015) 523–528. <http://dx.doi.org/10.1002/pssa.201400204>.
- [26] D. Ingerle, F. Meirer, G. Pepponi, E. Demenev, D. Giubertoni, P. Wobrauschek, C. Strelti, Combined evaluation of grazing incidence X-ray fluorescence and X-ray reflectivity data for improved profiling of ultra-shallow depth distributions, *Spectrochim. Acta B At. Spectrosc.* 99 (2014) 121–128. <http://dx.doi.org/10.1016/j.sab.2014.06.019>.
- [27] D. Ingerle, G. Pepponi, F. Meirer, P. Wobrauschek, C. Strelti, JGIXA: a software package for the calculation and fitting of grazing incidence X-ray fluorescence and X-ray reflectivity data for the characterization of nanometer-layers and ultra-shallow-implants, *Spectrochim. Acta B At. Spectrosc.* 118 (2016) 20–28. <http://dx.doi.org/10.1016/j.sab.2016.02.010>.
- [28] R. Storn, K. Price, Differential evolution: a simple and efficient heuristic for global optimization over continuous spaces, *J. Glob. Optim.* 11 (1997) 341–359.
- [29] H. Fujiwara, M. Kondo, Effects of carrier concentration on the dielectric function of ZnO:Ga and $\text{In}_2\text{O}_3:\text{Sn}$ studied by spectroscopic ellipsometry: analysis of free-carrier and band-edge absorption, *Phys. Rev. B* 71 (2005) 075109. <http://dx.doi.org/10.1103/PhysRevB.71.075109>.
- [30] J. Kim, G. Naik, A. Gavrilenko, K. Dondapati, V. Gavrilenko, S. Prokes, O. Glembocki, V. Shalaev, A. Boltasseva, Optical properties of gallium-doped zinc oxide - a low-loss plasmonic material: first-principles theory and experiment, *Phys. Rev X* 3 (2013) 041037. <http://dx.doi.org/10.1103/PhysRevX.3.041037>.
- [31] E. Burstein, Anomalous optical absorption limit in InSb, *Phys. Rev* 93 (1954) 632–633. <http://dx.doi.org/10.1103/PhysRev.93.632>.
- [32] B. Sernelius, K.-F. Berggren, Z.-C. Jin, I. Hamberg, C. Granqvist, Band-gap tailoring of ZnO by means of heavy Al doping, *Phys. Rev. B* 37 (1988) 10244–10248. <http://dx.doi.org/10.1103/PhysRevB.37.10244>.
- [33] J.I. Pankove, *Optical Processes in Semiconductors*, Dover Publication, 1975.
- [34] K. Ellmer, A. Klein, B. Rech, *Transparent conductive zinc oxide*, Vol. 104 of *Springer Series in Materials Science* Springer Berlin Heidelberg, 2007.
- [35] I. Hamberg, C. Granqvist, Evaporated Sn-doped In_2O_3 films: basic optical properties and applications to energy-efficient windows, *J. Appl. Phys.* 60 (1986) R123–R160. <http://dx.doi.org/10.1063/1.337534>.
- [36] J.C. Wong, C. Ortega, J. Siejka, I. Trimaille, A. Sacuto, L. Mercandalli, F. Mayca, Study of oxygen content and of disorder in YBaCuO thin films with enlarged c-axis lattice parameter, *J. Alloys Compd* 195 (1993) 675–678. [http://dx.doi.org/10.1016/0925-8388\(93\)90828-B](http://dx.doi.org/10.1016/0925-8388(93)90828-B).
- [37] H. Rotella, O. Copie, A. Pautrat, P. Boullay, A. David, D. Pelloquin, C. Labbé, C. Frilay, W. Prellier, Two components for one resistivity in $\text{LaVO}_3/\text{SrTiO}_3$ heterostructure, *Journal of Physics: Condensed Matter* 27 (9) (2015) 095603. <http://dx.doi.org/10.1088/0953-8984/27/9/095603>.
- [38] M. Kasik, C. Venzago, R. Dorka, Quantification in trace and ultratrace analyses using glow discharge techniques: round robin test on pure copper materials, *J. Anal. At. Spectrom.* 18 (2003) 603–611. <http://dx.doi.org/10.1039/B300025G>.
- [39] D. Lide, *CRC Handbook of Chemistry and Physics*, 85th ed., CRC press, 2004.